crystals

MDPI

Communication

Performance Analysis of DAST Material-Assisted Photonic-Crystal-Based Electrical Tunable Optical Filter

Amit Kumar Goyal [1], Ajay Kumar [2] and Yehia Massoud [1,*]

[1] Innovative Technologies Laboratories (ITL), King Abdullah University of Science and Technology (KAUST), Thuwal 23955, Saudi Arabia; amit.goyal@kaust.edu.sa
[2] ECE Department, Jaypee Institute of Information Technology, Noida 201309, India; ajay.kumar@jiit.ac.in
* Correspondence: yehia.massoud@kaust.edu.sa

Abstract: In this paper, a 4-*N*,*N*-dimethylamino-4′-*N*′-methyl-stilbazolium tosylate (DAST) material assisted one-dimensional photonic-crystal-based (1D-PhC) tunable optical filter is presented. The design comprises a bilayer 1D-PhC structure having DAST as an electro-optic material. The device parameters are configured to filter out the 632.8 nm wavelength from the reflection spectrum. The analysis shows that by illuminating the device with poly-chromatic light at an incident angle of 45.07°, the filtered wavelength exhibits transmission maxima having FWHM of less than 1nm. The analytical results also demonstrate the post fabrication 60 nm electrical tuning of the filtered wavelength by using only ±5 V applied potential. The structure also exhibits a very stable filter response up to 40% variations in optical thickness. Thus, the proposed design possesses the advantage in terms of low voltage wavelength tuning, stable response, easy fabrication and integration capability in integrated circuits.

Keywords: optical filter; electrical tunable; DAST material; one-dimensional photonic crystal

Citation: Goyal, A.K.; Kumar, A.; Massoud, Y. Performance Analysis of DAST Material-Assisted Photonic-Crystal-Based Electrical Tunable Optical Filter. *Crystals* **2022**, *12*, 992. https://doi.org/10.3390/cryst12070992

Academic Editors: Muhammad Ali Butt and Svetlana Nikolaevna Khonina

Received: 24 June 2022
Accepted: 15 July 2022
Published: 17 July 2022

Publisher's Note: MDPI stays neutral with regard to jurisdictional claims in published maps and institutional affiliations.

1. Introduction

Post fabrication tuning of the optical properties of the surface wave-based nano-photonic systems working in the visible region are attracting wide attention particularly to develop reconfigurable optical devices [1,2]. The optical properties and surface wave responses of the nano-photonic devices can be dynamically tuned by considering an external stimulus. This requires the integration of functional materials such as electro-optical (EO) materials [3–5], thermo-optical (TO) materials and phase change (PCM) materials [6–9] with conventional surface wave-based devices [10–14]. Additionally, the integrated material should possess a correspondingly large coefficient of variations. This enables developing a number of tunable surface wave-based nano-photonic devices [15–17]. Recently, tunable narrowband spectral filters have gained considerable attention because of their wide applications in spectroscopy, imaging, sensing, smart display and astronomy [18–23]. In 2022, Chen et al. [24], developed a graphene-based electrical tunable filter and observed a 1.62 nm wavelength tuning by applying a maximum voltage of 30 V. The $Ge_2Sb_2Se_2Te_1$ (GSST) phase change material has been explored in a metal–insulator–metal (MIM) configuration to completely reject the 850 nm wavelength range [25]. The epsilon-near-zero (ENZ) material (n doped-InSb) has also been explored in a Fabry–Pérot nanocavity configuration to tune the absorbance wavelength in the visible region. The authors reported a 40 nm tuning (625–665 nm) for an applied maximum voltage of 50 V [26]. A distributed Bragg reflector-based (DBR) optical filter working as an alternative to the well-known Fabry–Pérot filters for a NIR region is proposed by Ahmed et al. [27] and the authors reported a FWHM of around 0.016 of filtered wavelength. A similar structure working on a guided-mode resonance principal is also explored to work as a Fano filter device [28]. In most of the reported works, either wavelength tuning range is very low or one needs to apply a very

large voltage. Additionally, the full-width-half-maximum (FWHM) of filtered wavelength is very large, thus not widely applicable in fine spectral tuning applications.

Recently, an organic crystal 4-*N*,*N*-dimethylamino-4′-*N*′-methyl-stilbazolium tosylate (DAST) as an EO material [29] has been widely explored for various high-speed electro-optic applications and THz-wave generation [30,31]. It is also explored to design an all weather electro-tunable smart window [32] and a tunable color filter in an MIM cavity configuration using silver [33]. In this article, a simple approach has been proposed to design a dynamical tunable optical filter. This comprises utilizing a DAST as an EO material [29], to be incorporated in a multilayer structure to electrically tune the reflection spectrum. DAST has a very large EO coefficient of around 3.41 nm/V, which is more suitable for electrical tuning purposes compared to a standard $LiNbO_3$ material [34]. The design optimization and structural analysis is carried out using both the finite element method (FEM) and the transfer matrix method (TMM). The detailed optimization of the device results in selective transmission of a specific wavelength having very narrow FWHM. The analysis is carried out to measure the transmission wavelength tuning with respect to the applied voltage. This shows that by illuminating the device with polychromatic light at an incident angle of 45.07°, the filtered wavelength exhibits transmission maxima having FWHM of less than 1nm. Furthermore, the results also demonstrate the post fabrication 60 nm electrical tuning of filter wavelength by using only ±5 V applied potential. The proposed design possesses the advantage in terms of low voltage wavelength tuning, easy fabrication and integration capability in integrated circuits having possible applications in dynamic displays, colour tunable smart windows, tunable switches and imaging devices. The novel 1D-PhC and EO material integration further strengthens its competency and inspires for the future scope.

2. Design Methodology and Optimization

The proposed structure works on the basis of DBR. It is designed by considering DAST and SiO_2 as the high and low refractive index (RI) materials. The total thickness of the structure is only around 1691 nm, where the thickness of the layers (DAST, and SiO_2) is 85 and 128 nm from the bottom substrate to the top. The structure is terminated by a low index defect layer of 200 nm thickness followed by surrounding medium (here, air) of 1000 nm thickness. The thickness values are optimized to filter out wavelengths of interest (initially 632.8 nm). This is attained by satisfying the phase-matching condition of the incident light, which is accomplished by using a BK7 glass prism arranged in a Kretschmann configuration [35,36].

The schematic of the proposed structure 'substrate | $(SiO_2$,DAST$)^7$ | SiO_2 | air' and its corresponding 2-dimensional (2D) electric field profile is presented in Figure 1. The structure analysis was carried out to calculate the reflection, absorption and transmission spectrum. The structure comprises 7 pairs of DAST/SiO_2 layers arranged in a Bragg stack configuration to obtain overall high reflectivity as shown in Figure 1a. Here, substrate and SiO_2 are considered having RI of about 1.515, and 1.45, respectively. The absorption property of SiO_2 has also been taken care of by considering 0.0001i as the imaginary part of the dielectric constant. The optical constant values for DAST are taken from [37]. Figure 1b represents the 2D surface electric filed profile of the proposed structure 'substrate | $(SiO_2$,DAST$)^7$ | SiO_2 | air'. Here, the light is incident in 'z' direction. Thus, the electric field profile within each layer can be calculated by [38–40] Equation (1).

$$E(z,x) = A_n e^{ik_n z} + B_n e^{-ik_n z} = A(z) + B(z) \quad (1)$$

where $A(z)$ represents the forward propagating field, and $B(z)$ represents the backward propagating field components having corresponding field amplitudes as A_n and B_n. The field amplitudes are computed for every nth layer by using the transfer matrix method (TMM). This provides a direct relation between incident and reflected wave amplitudes for a finite size proposed structure and given by Equation (2).

$$\begin{pmatrix} A_{n-1} \\ B_{n-1} \end{pmatrix} = M_n \begin{pmatrix} A_n \\ B_n \end{pmatrix} = \begin{pmatrix} M11 & M12 \\ M21 & M22 \end{pmatrix} \begin{pmatrix} A_n \\ B_n \end{pmatrix} \quad (2)$$

Since the structure is periodic in nature, the eigenvalue equation is formulated by applying the Floquet theorem, which is further solved to obtain the reflection, transmission and absorption response of the proposed structure [41,42].

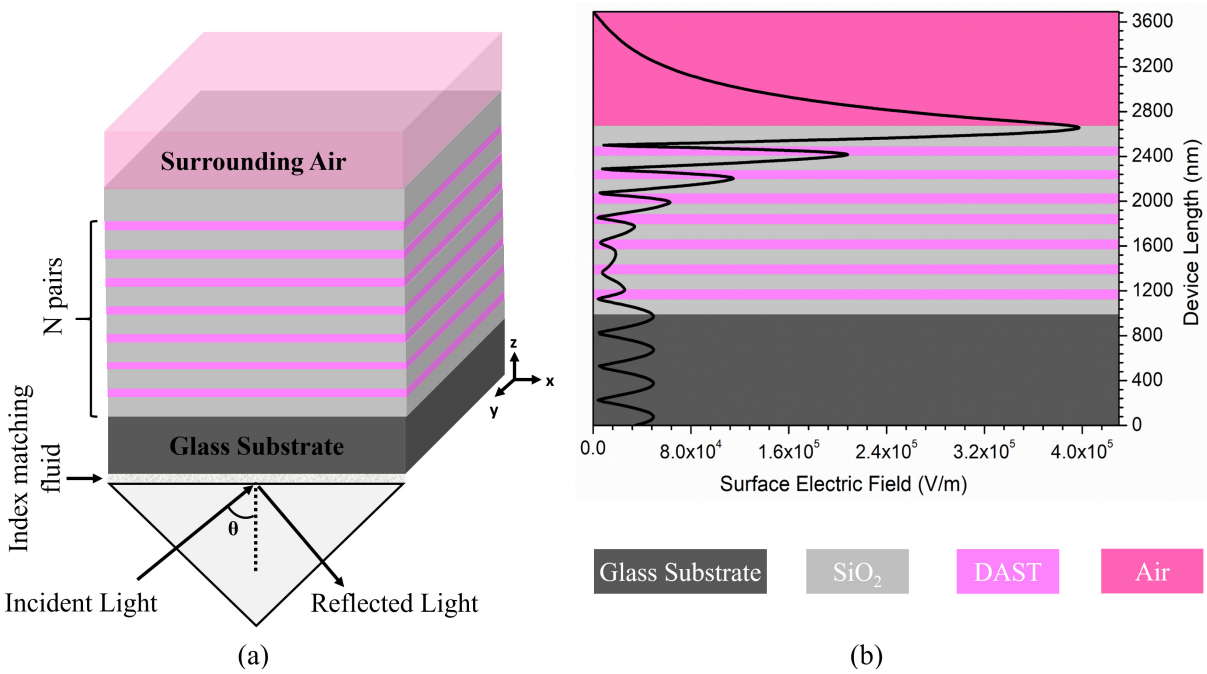

Figure 1. (**a**) Schematic of proposed filter structure and (**b**) corresponding surface electric field profile at a central wavelength of 632.8 nm and incident angle of 45.07°.

3. Simulation Results and Discussion

Initially, the analysis is carried out by calculating both the angular and wavelength-dependent reflectance spectrum of the proposed device. Figure 2a represents the reflectivity spectrum with respect to the incident angle at a fixed central operating wavelength of 632.8 nm.

A simple DBR structure comprises 'substrate | $(SiO_2,DAST)^7$ | air', whereas a DBR with a defect layer is made of a 'substrate | $(SiO_2,DAST)^7$ | SiO_2 | air' configuration. The simple DBR structure works as a dielectric mirror; thus a broadband spectrum is reflected. However, the incorporation of a defect layer on the proposed structure results in filtration of a 632.8 nm wavelength from the reflection spectrum at a 45.07° incident angle. Thus, the angular interrogation exhibits the filtration of a 632.8 nm wavelength from the reflection spectrum at an incident angle of 45.07°. This is because the dispersion curve for the surface mode comes near the air–light line and is represented by the red curve of Figure 2a. This is further verified by calculating the wavelength-dependent reflection spectrum of the proposed structure 'substrate | $(SiO_2,DAST)^7$ | SiO_2 | air' and is represented in Figure 2b. It is clear from Figure 2b that for a fixed incident angle of 45.07°, the structure reflects all the incident wavelength spectrum except at 632.8 nm. Thus, a sharp dip corresponding to the 632.8 nm wavelength is observed, which confirms that the mentioned wavelength is filtered out from the reflection spectrum. Additionally, the structure can further be optimized to filter out any other desired wavelength by tuning the optical length of the considered materials as shown in Figure 3. Figure 3a represents the impact of varying DAST material thickness on a filtered wavelength at a fixed incidence angle of 45.07°.

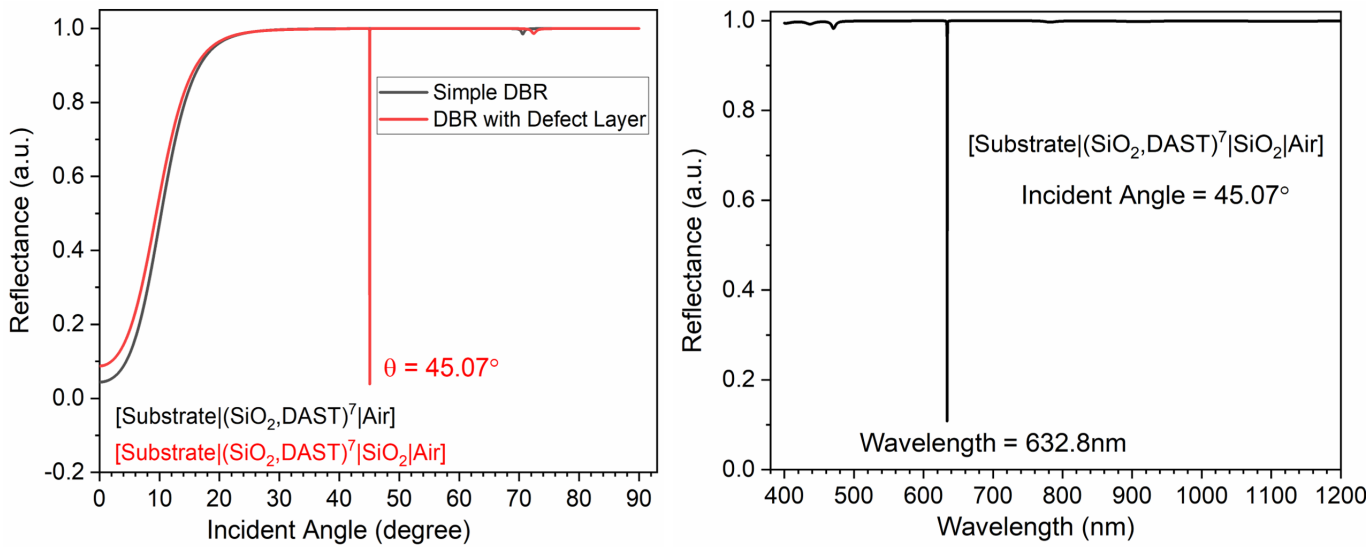

Figure 2. Reflectivity analysis of the designed structure: (**a**) effect of the incident angle on the reflectivity spectrum for a simple DBR (substrate | $(SiO_2,DAST)^7$ | air) and a DBR with a defect layer (substrate | $(SiO_2,DAST)^7$ | SiO_2 | air) at 632.8 nm incident wavelength; (**b**) wavelength interrogation of the (substrate | $(SiO_2,DAST)^7$ | SiO_2 | air) structure at a 45.07° incident angle.

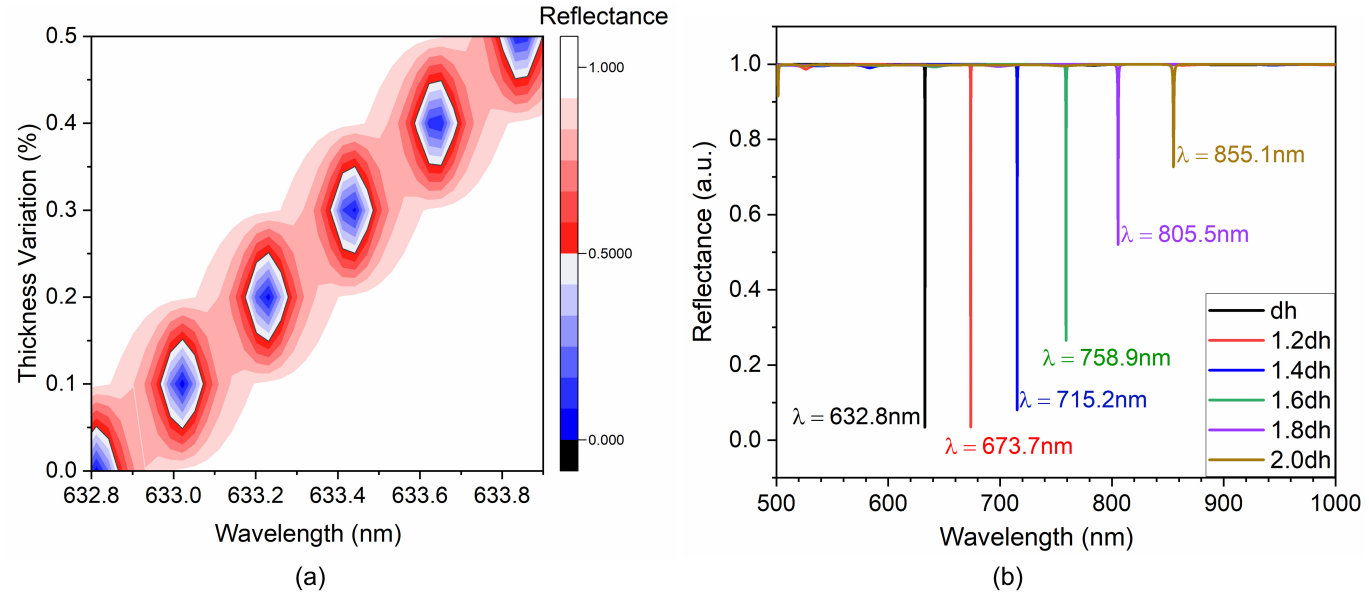

Figure 3. The impact of varying DAST material width on filtered wavelength for a constant incidence angle of 45.07:° (**a**) for 0.5% thickness variation; and (**b**) for 100% thickness variation.

Increasing DAST material thickness only 0.5% results in around a 1 nm change in the filtrated wavelength. Moreover, the transmission intensity of the infiltrated wavelength is very high (blue colour in the centre), and the FWHM (black circle width) is only around 0.1 nm, which is more suitable for fine spectral tuning applications. Additionally, the proposed design concept is further extended for broad spectral tuning of the filtered wavelength, and it is observed that the structure possesses very good filter wavelength tuning as shown in Figure 3b. Increasing the DAST material thickness from dh to 2 dh in the step of 20%, results in filtration of 632.8 nm, 673.73 nm, 715.29 nm, 758.97 nm, 805.53 nm and 855.12 nm wavelengths, respectively. The structure exhibits around 82.4 nm (632.8 nm to 715.2 nm) wavelength tuning having strong reflection minima for a corresponding 40%

increase in DAST material thickness. The same has been summarized in Table 1. However, the thickness variations can also occur because of fabrication imperfection, which results in undesirable filtered wavelength tuning. This problem can be alleviated, and the structure can be made to filter a fixed wavelength at different incidence angles. Thus, the analysis is further extended to calculate the impact of varying DAST material thickness on required incidence angles to filter out a fixed operating wavelength of 632.8 nm. Figure 4 represents the impact of varying DAST material thickness on the incidence angle for a fixed operating wavelength of 632.8 nm. Increasing DAST material thickness only 0.5% results in around a 0.13% change in the incidence angle to filter-out a 632.8 nm wavelength. Moreover, the reflected intensity of the infiltrated wavelength is very low (blue colour in the centre).

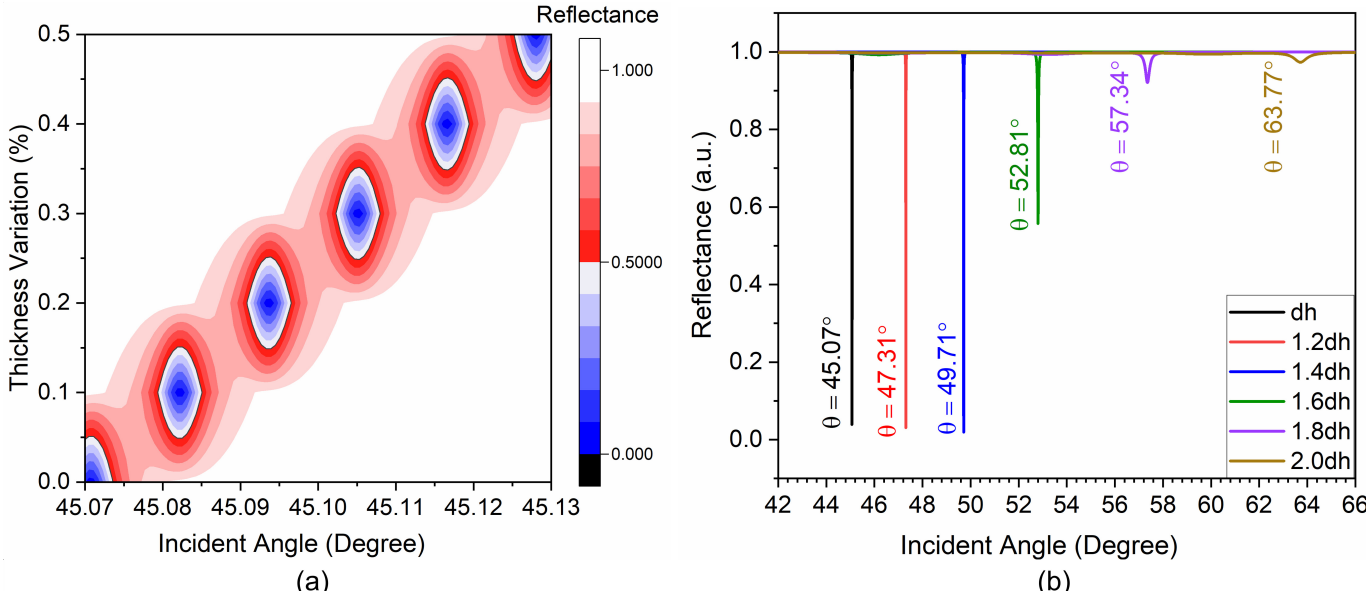

Figure 4. The impact of varying the DAST material width on the required incidence angle to filter out a constant wavelength of 632.8 nm: (**a**) for 0.5% thickness variation; and (**b**) for 100% thickness variations.

The analysis is further extended to higher thickness variations, and it is observed that the structure possesses a very stable filtered wavelength response as shown in Figure 4b. Increasing the DAST material thickness from dh to 2 dh in the step of 0.2 results in filtration of a 632.8 nm wavelength at corresponding incidence angles of 45.07°, 47.31°, 49.71°, 52.81°, 57.34° and 63.77°, respectively. The structure requires around 10.3% variations in incidence angle to filter a 632.8 nm wavelength for a corresponding 40% increase in DAST material thickness. Increasing the DAST material thickness beyond 40% results in higher top interface losses. These results have been summarized in Table 1. The analysis shows that the proposed device has very good fabrication tolerance as the wavelength filtration will still occur even after a small variation in fabrication parameters.

Table 1. Effect of thickness variation on both incidence angle and excitation wavelength.

Thickness Variation	Incident Angle at Fixed Wavelength of 632.8 nm	Filtered Wavelength at Fixed Angle of 45.07°
1.0 × dh	45.07 °C	632.80 nm
1.2 × dh	47.31 °C	673.73 nm
1.4 × dh	49.71 °C	715.29 nm
1.6 × dh	52.81 °C	758.97 nm
1.8 × dh	57.34 °C	805.53 nm
2.0 × dh	63.77 °C	855.12 nm

Since many times, post-fabrication device tuning is required, the electro-optical (EO) property of the DAST material is considered. Once the device is fabricated and layer thicknesses are measured, voltage at the DAST material can be applied to tune its wavelength filtration characteristics. DAST possesses a very high EO coefficient (3.41 nm/V), which is sufficient enough to tune the operating wavelength with minimum bias voltage [43–45]. Since the EO coefficient of SiO_2 is very small it does not have any much impact on the analysis. The EO coefficient and the corresponding refractive index variation of DAST is calculated by Equation (3) [33].

$$nH = n' + \frac{dn}{du}\frac{V}{th} \tag{3}$$

where n' is the RI of material at zero applied voltage, dn/du is the EO coefficient considered as 3.4 (nm/V), 'V' is the applied voltage, and 'th' is the layer thickness measured after fabrication. The 'th' value can be obtained by either scanning electron microscopy (SEM) imaging or spectroscopy ellipsometry measurement.

Figure 5a represents the impact of applying small bias voltage (0–0.5 V) on the reflectance characteristic of the proposed structure 'substrate | $(SiO_2$,DAST$)^7$ | SiO_2 | air'. Increasing the bias voltage from 0 to 0.5 V results in an increase in 3nm variation in filtered wavelength. Additionally, the transmission intensity of the infiltrated wavelength is very high (blue colour in the centre), and the FWHM (black circle width) is only around 0.1 nm, thus retaining its fine spectral tuning characteristic. Figure 5b represents the extended analysis for higher applied voltages, and it is observed that the structure possesses very good filtered wavelength tuning. Increasing the applied bias voltage from −5 V, −2.5 V, 0 V, 2.5 V and 5 V results in transmission maxima at corresponding wavelengths of 598.9 nm, 617.0 nm, 632.8 nm, 646.7 nm and 659.2 nm, respectively. The structure exhibits around 60 nm wavelength tuning for a corresponding ±5 V applied bias voltage.

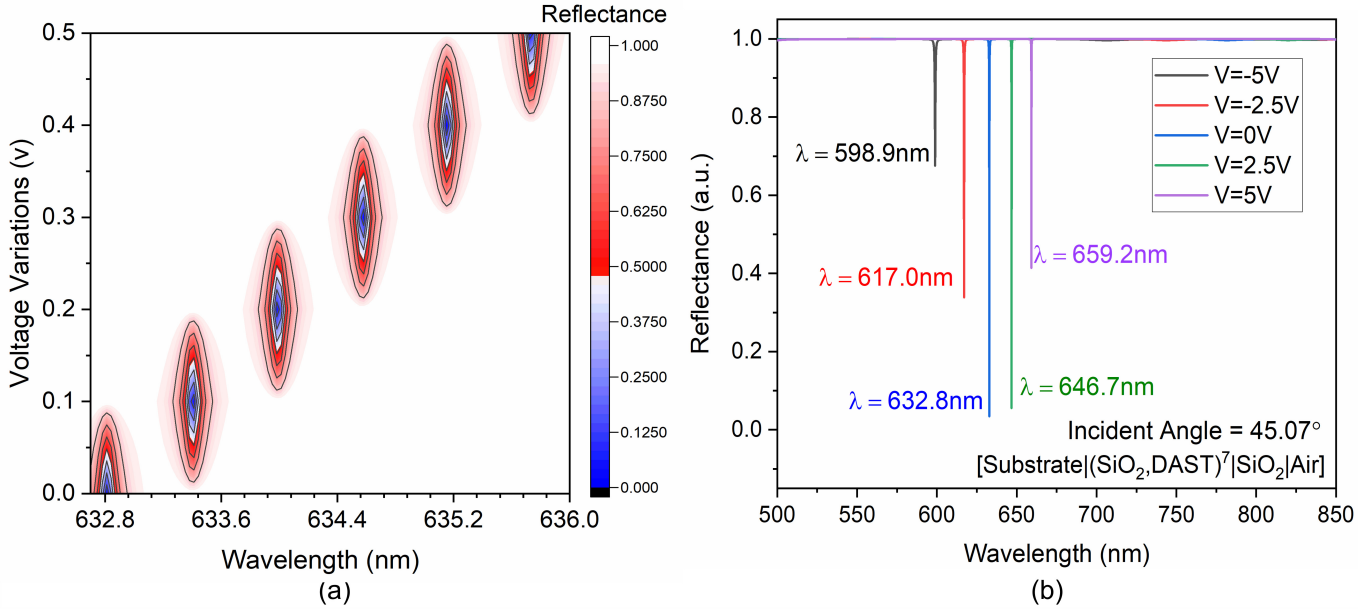

Figure 5. The wavelength-dependent reflectance spectrum at a fixed incidence angle of 45.07° for applied voltage of: (**a**) 0 V to 0.5 V; (**b**) for −5.0 V to 5.0 V.

Figure 6 represents the filtered wavelength stability analysis at different applied voltage. Figure 6a represents the impact of varying applied bias voltage on the incidence angle for a fixed operating wavelength of 632.8 nm. Increasing only 0.5 V bias voltage results in around a 0.35% change in the incidence angle to filter the 632.8 nm wavelength. The analysis is further extended to higher applied bias voltage, and it is observed that the structure possesses a very stable filtered wavelength response as shown in Figure 6b.

Increasing the bias voltage from −5 V to 5 V in the step of 2.5 V, results in filtration of the 632.8 nm wavelength at corresponding incidence angles of 42.98°, 44.15°, 45.07°, 45.81° and 46.43°, respectively. The structure requires around 1.64% variations in incidence angle to filter a 632.8 nm wavelength for a corresponding 2.5 V increase in applied bias voltage. These results have been summarized in Table 2.

Table 2. Effect of applied voltage on both incidence angle and excitation wavelength.

Bias Voltage	Angular Interrogation		Wavelength Interrogation	
	Incidence Angle	FWHM	Resonance Wavelength	FWHM
−5.0	42.98 °C	0.06 °C	598.9 nm	0.45 nm
−2.5	44.15 °C	0.007 °C	617.0 nm	0.18 nm
0	45.07 °C	0.006 °C	632.8 nm	0.11 nm
2.5	45.81 °C	0.004 °C	646.7 nm	0.07 nm
5.0	46.43 °C	0.005 °C	659.2 nm	0.08 nm

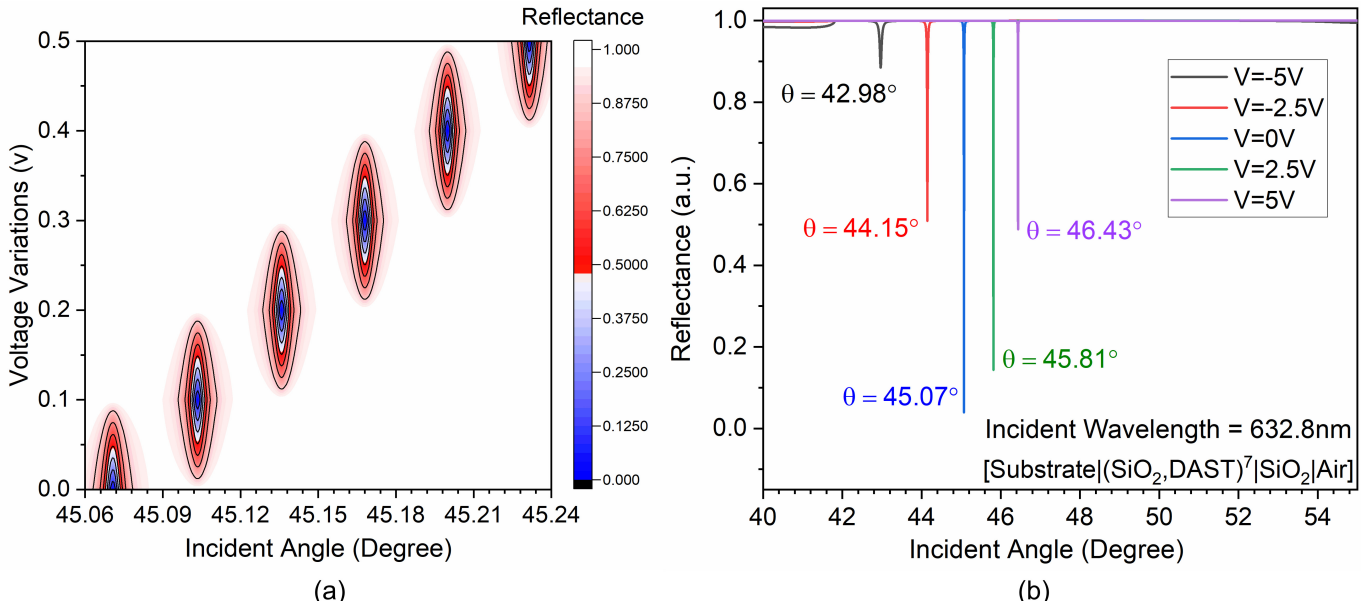

Figure 6. The impact of voltage variation on the reflectance spectrum for a constant incident wavelength of 632.8 nm at an applied voltage of: (**a**) 0 V to 0.5 V; and (**b**) for −5.0 V to 5.0 V.

Figure 7 summarizes the post-fabrication voltage-dependent filter wavelength tuning capability of the structure for both fixed filtered wavelength and fixed incidence angle. The structural voltage-dependent filter wavelength tuning response can be measured by Equation (4), and the corresponding wavelength stability is calculated by Equation (5).

$$\lambda = 632.8 + 6.012V - 0.1497V^2 \quad (4)$$

$$\theta = 45.07 + 0.3424V - 0.1463V^2 \quad (5)$$

It is clearly evident from the graph that the bias-voltage-dependent filter wavelength (at a fixed incidence angle of 45.07°) and incidence angles (at fixed operating wavelength of 632.8 nm) show a good polynomial relation with the coefficients of determination R^2 which are 0.99918 and 0.97546, respectively. Therefore, the proposed structure shows its capability as an angular wavelength filter having its potential applications in dynamic displays, colour tunable smart windows, tunable switches and imaging devices. Moreover, the structure can be fabricated by a simple spin/dip coating or deposition method, thus eliminating the need of complex fabrication techniques [46–48]. The novel 1D-PhC and EO material integration further strengthens its competency and inspires for the future scope.

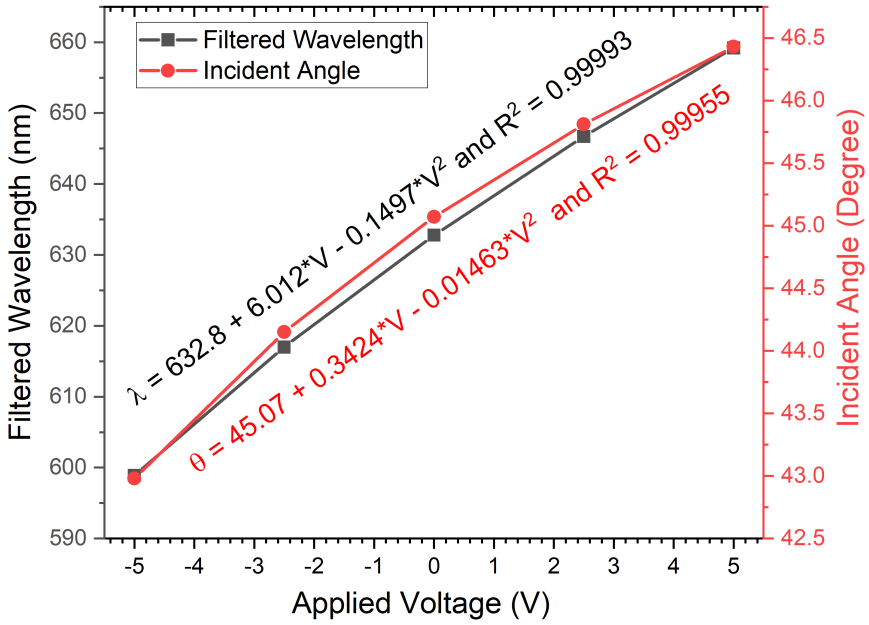

Figure 7. The comparative representation of the applied voltage on the filter wavelength at a constant incidence angle of 45.07° and on an incidence angle at a fixed filter wavelength of 632.8 nm.

4. Conclusions

In this paper, a 1D-PhC-based electrically tunable optical filter is presented. The design comprises SiO_2 as a low refractive index material and DAST as a high refractive index material having an EO coefficient of around 3.41 nm/V. The structural analysis demonstrates a very stable filter response for a filtered wavelength of 632.8 nm. Additionally, the filtered wavelengths and incidence angles can also be tuned to a desired user-defined value. The theoretical results indicate that the centre wavelength of the proposed filter structure can be tuned over the broad range of about 60 nm for a ±5 V applied potential having FWHM of less than 1 nm. The proposed structure is a promising candidate in the field of dynamic displays, colour tunable smart windows, tunable switches, and imaging devices because of its remarkable performance characteristics such as fine wavelength tunability, higher stability and minimum FWHM.

Author Contributions: Conceptualization, A.K.G., A.K. and Y.M.; formal analysis, A.K.G. and A.K.; investigation, Y.M.; methodology, A.K.G.; supervision, Y.M.; validation, A.K.; writing—original draft, A.K.G. and A.K.; writing—review and editing, Y.M. All authors have read and agreed to the published version of the manuscript.

Funding: The authors would like to acknowledge the research funding to the Innovative Technologies Laboratories (ITL) from King Abdullah University of Science and Technology (KAUST).

Institutional Review Board Statement: Not applicable.

Informed Consent Statement: Not applicable.

Data Availability Statement: Data underlying the results presented in this paper are not publicly available at this time but may be obtained from the authors upon reasonable request.

Conflicts of Interest: The authors declare no conflict of interest.

References

1. Neubrech, F.; Duan, X.; Liu, N. Dynamic plasmonic color generation enabled by functional materials. *Sci. Adv.* **2020**, *6*, eabc2709. [CrossRef] [PubMed]
2. Duan, X.; Liu, N. Magnesium for dynamic nanoplasmonics. *Acc. Chem. Res.* **2019**, *52*, 1979–1989. [CrossRef] [PubMed]
3. Sharma, M.; Hendler, N.; Ellenbogen, T. Electrically switchable color tags based on active liquid-crystal plasmonic metasurface platform. *Adv. Opt. Mater.* **2020**, *8*, 1901182. [CrossRef]

4. Shahabuddin, M.; McDowell, T.; Bonner, C.E.; Noginova, N. Enhancement of electrochromic polymer switching in plasmonic nanostructured environment. *ACS Appl. Nano Mater.* **2019**, *2*, 1713–1719. [CrossRef]
5. Aly, A.H.; Sayed, F.A.; Hussein, A.E. Defect mode tunability based on the electro-optical characteristics of the one-dimensional graphene photonic crystals. *Appl. Opt.* **2020**, *59*, 4796–4805. [CrossRef]
6. Wuttig, M.; Bhaskaran, H.; Taubner, T. Phase-change materials for non-volatile photonic applications. *Nat. Photonics* **2017**, *11*, 465. [CrossRef]
7. Jeong, H.D.; Lee, S.Y. Tunable plasmonic absorber using a nano slit array patterned on a Ge2Sb2Te5-inserted Fabry–Perot resonator. *J. Light. Technol.* **2018**, *36*, 5857–5862. [CrossRef]
8. Zhao, Z. Sn dopants improve the visible transmittance of VO2 films achieving excellent thermos-chromic performance for smart window. *Sol. Energy Mater. Sol. Cells* **2020**, *209*, 110443. [CrossRef]
9. Alam, M.; Massoud, Y. RLC ladder model for scattering in single metallic nanoparticles. *IEEE Trans. Nanotechnol.* **2006**, *5*, 491–498. [CrossRef]
10. Goyal, A.K.; Saini, J. Performance Analysis of Bloch Surface Wave Based Sensor using Transition Metal Dichalcogenides. *Appl. Nanosci.* **2020**, *10*, 4307–4313. [CrossRef]
11. Meade, R.D.; Brommer, K.D.; Rappe, A.M.; Joannopoulos, J.D. Electromagnetic Bloch waves at the surface of a photonic crystal. *Phys. Rev. B* **1991**, *44*, 10961. [CrossRef] [PubMed]
12. Dutta, H.S.; Goyal, A.K.; Pal, S. Analysis of Dispersion Diagram for High Performance Refractive Index Sensor based on Photonic Crystal Waveguides. *Photonics Nanostruct.* **2017**, *23*, 21–27. [CrossRef]
13. Robertson, W.M.; Arjavalingam, G.; Meade, R.D.; Brommer, K.D.; Rappe, A.M.; Joannopoulos, J.D. Observation of surface photons on periodic dielectric arrays. *Opt. Lett.* **1993**, *18*, 528–530. [CrossRef] [PubMed]
14. Goyal, A.K.; Kumar, A.; Massoud, Y. Thermal Stability Analysis of Surface Wave Assisted Bio-Photonic Sensor. *Photonics* **2022**, *9*, 324. [CrossRef]
15. Duan, X.; Kamin, S.; Liu, N. Dynamic plasmonic colour display. *Nat. Commun.* **2017**, *8*, 14606. [CrossRef]
16. Xiong, K.; Tordera, D.; Jonsson, M.P.; Dahlin, A.B. Active control of plasmonic colors: Emerging display technologies. *Rep. Prog. Phys.* **2019**, *82*, 024501. [CrossRef]
17. Damgaard-Carstensen, C.; Thomaschewski, M.; Ding, F.; Bozhevolnyi, S.I. Electrical Tuning of Fresnel Lens in Reflection. *ACS Photonics* **2021**, *8*, 1576–1581. [CrossRef]
18. Gat, N. Imaging spectroscopy using tunable filters: A review. *Proc. SPIE* **2000**, *4056*, 50–64.
19. Ebermann, M.; Neumann, N.; Hiller, K.; Seifert, M.; Meinig, M.; Kurth, S. Tunable MEMS Fabry-Pérot filters for infrared micro spectrometers: A review. *Proc. SPIE* **2016**, *9760*, 97600H1-20.
20. Gebhart, S.C.; Thompson, R.C.; Mahadevan-Jansen, A. Liquid crystal tunable filter spectral imaging for brain tumor demarcation. *Appl. Opt.* **2007**, *46*, 1896–1910. [CrossRef]
21. Hosseini, A.; Massoud, Y. Optical range microcavities and filters using multiple dielectric layers in metal-insulator-metal structures. *J. Opt. Soc. Am. A* **2007**, *24*, 221–224. [CrossRef] [PubMed]
22. Ratra, K.; Singh, M.; Goyal, A.K. Design and Analysis of Omni-directional Solar Spectrum Reflector using One-dimensional Photonic Crystal. *J. Nanophotonics* **2020**, *14*, 026005. [CrossRef]
23. Hosseini, A.; Nejati, H. Massoud, Y. Design of a maximally flat optical low pass filter using plasmonic nanostrip waveguides. *Opt. Express* **2007**, *15*, 15280–15286. [CrossRef] [PubMed]
24. Chen, Q.; Gao, F.; Wang, D.N.; Wang, Z.; Wang, Y. Electrically tunable optical filter based on tapered fiber coated with porous graphene film. *Opt. Commun.* **2022**, *505*, 127518. [CrossRef]
25. Heenkenda, R.; Hirakawa, K.; Sarangan, A. Tunable optical filter using phase change materials for smart IR night vision applications. *Opt. Express* **2021**, *29*, 33795–33803. [CrossRef]
26. Mirshafieyan, S.S.; Gregory, D.A. Electrically tunable perfect light absorbers as color filters and modulators. *Sci. Rep.* **2018**, *8*, 2635. [CrossRef]
27. Ahmed, U.; Khan, Y.; Ehsan, M.K.; Amirzada, M.R.; Ullah, N.; Khatri, A.R.; Ur Rehman, A.; Butt, M.A. Investigation of Spectral Properties of DBR-Based Photonic Crystal Structure for Optical Filter Application. *Crystals* **2022**, *12*, 409. [CrossRef]
28. Khan, Y.; Rehman, A.U.; Batool, B.A.; Noor, M.; Butt, M.A.; Kazanskiy, N.L.; Khonina, S.N. Fabrication and Investigation of Spectral Properties of a Dielectric Slab Waveguide Photonic Crystal Based Fano-Filter. *Crystals* **2022**, *12*, 226. [CrossRef]
29. Marder, S.R.; Perry, J.W.; Schaefer, W.P. Synthesis of organic salts with large 2nd-order optical nonlinearities. *Science* **1989**, *245*, 626–628. [CrossRef]
30. Vicario, C.; Jazbinsek, M.; Ovchinnikov, A.V.; Chefonov, O.V.; Ashitkov, S.I.; Agranat, M.B.; Hauri, C.P. High efficiency THz generation in DSTMS, DAST and OH1 pumped by Cr: Forsterite laser. *Opt. Express* **2015**, *23*, 4573–4580. [CrossRef]
31. Stepanov, A.G.; Bonacina, L.; Wolf, J. DAST/SiO_2 multilayer structure for efficient generation of 6 THz quasi-single-cycle electromagnetic pulses. *Opt. Lett.* **2012**, *37*, 2439–2441. [CrossRef] [PubMed]
32. Chowdhary, A.; Sikdar, D. Design of electrotunable all-weather smart windows. *Sol. Energy Mater. Sol. Cells* **2021**, *222*, 110921. [CrossRef]
33. Aalizadeh, M.; Serebryannikov, A.E.; Khavasi, A.; Vandenbosch, G.; Ozbay, E. Toward Electrically Tunable, Lithography-Free, Ultra-Thin Color Filters Covering the Whole Visible Spectrum. *Sci. Rep.* **2018**, *8*, 11316. [CrossRef] [PubMed]

34. Jazbinsek, M.; Mutter, L.; Gunter, P. Photonic applications with the organic nonlinear optical crystal DAST. *IEEE J. Sel. Top. Quantum Electron.* **2**008, *14*, 1298–1311. [CrossRef]
35. Robertson, W.M. Experimental Measurement of the Effect of Termination on Surface Electromagnetic Waves in One-Dimensional Photonic Bandgap Arrays. *J. Light. Technol.* **1999**, *17*, 2013. [CrossRef]
36. Li, Y. Phase properties of Bloch surface waves and their sensing applications. *Appl. Phys. Lett.* **2013**, *103*, 041116. [CrossRef]
37. Wang, Z.; Zhou, P.; Zheng, G. Electrically switchable highly efficient epsilon-near zero metasurfaces absorber with broadband response. *Results Phys.* **2019**, *14*, 102376. [CrossRef]
38. Pochi, Y. Electromagnetic propagation in periodic stratified media I. General theory. *J. Opt. Soc. Am.* **1977**, *67*, 423–438.
39. Hosseini, A.; Nejati, H.; Massoud, Y. Triangular lattice plasmonic photonic band gaps in subwavelength metal-insulator-metal waveguide structures. *Appl. Phys. Lett.* **2008**, *92*, 013116. [CrossRef]
40. Goyal, A.K. Design Analysis of One-dimensional Photonic Crystal Based Structure for Hemoglobin Concentration Measurement. *Prog. Electromagn. Res. M* **2020**, *97*, 77–86. [CrossRef]
41. Goyal, A.K.; Dutta, H.S.; Pal, S. Porous photonic crystal structure for sensing applications. *J. Nanophotonics* **2018**, *12*, 040501. [CrossRef]
42. Hosseini, A.; Nieuwoudt, A.; Massoud, Y. Efficient simulation of subwavelength plasmonic waveguides using implicitly restarted Arnoldi. *Opt. Exp.* **2006**, *14*, 7291–7298. [CrossRef] [PubMed]
43. Zhu, Y.J.; Huang, X.G.; Mei, X. A Surface Plasmon Polariton Electro-Optic Switch Based on a Metal-Insulator-Metal Structure with a Strip Waveguide and Two Side-Coupled Cavities. *Chin. Phys. Lett.* **2012**, *29*, 064214. [CrossRef]
44. Taheri, A.N.; Kaatuzian, H. Numerical investigation of a nano-scale electro-plasmonic switch based on metal-insulator-metal stub filter. *Opt. Quant. Electron.* **2015**, *47*, 159–168. [CrossRef]
45. Guo, J.J. Electrically Tunable Gap Surface Plasmon-based Metasurface for Visible Light. *Sci. Rep.* **2017**, *7*, 14078. [CrossRef]
46. Goyal, A.K.; Kumar, A. Recent advances and progresses in photonic devices for passive radiative cooling application: A review. *J. Nanophotonics* **2020**, *14*, 030901. [CrossRef]
47. Goyal, A.K.; Dutta, H.S.; Singh, S.; Kaur, M.; Husale, S.; Pal, S. Realization of Large-Scale Photonic Crystal Cavity-Based Devices. *J. Micro/Nanolith. Mems Moems* **2016**, *15*, 031608. [CrossRef]
48. Goyal, A.K.; Dutta, H.S.; Pal, S. Development of Uniform Porous One-dimensional Photonic Crystal Based Sensor. *Optik* **2020**, *223*, 165597. [CrossRef]